Cell

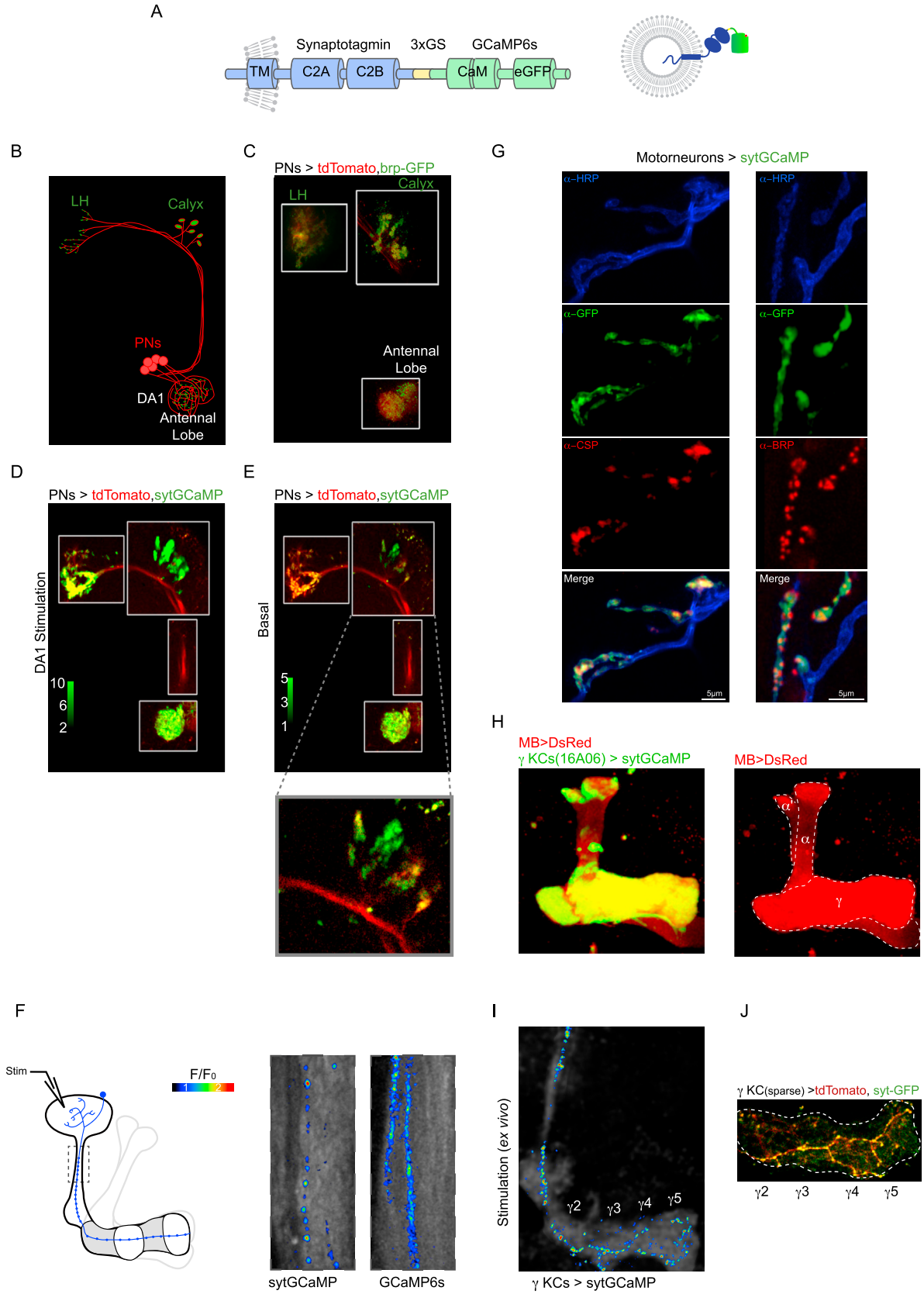

(legend on next page)

Figure S1. sytGCaMP, A Synaptically Localized Ca^{2+} Indicator, Highlights Functional γ KC Synapses throughout the Lobe, Related to Figure 1

(A) Schematic of the sytGCaMP construct (left) showing protein domains of synaptotagmin (blue) and GCaMP6s (green), including membrane-spanning portion of synaptotagmin (TM) and a GS-repeat linker (yellow). Schematic of sytGCaMP orientation placing the sensor outside the lumen of a synaptic vesicle (right).

(B) Schematic of antennal lobe projection neurons (PNs are red, presynaptic sites in green) labeled by MZ19-Gal4. PNs receive excitatory input and synapse onto interneurons in the antennal lobe glomeruli (including DA1). They project axons into the mushroom body calyx, where they form *en passant* synaptic boutons and then terminate in the lateral horn (LH).

(C) MZ19+ neurons are labeled red with the the fluorophore, tdTomato, and their synapses labeled green with GFP-tagged presynaptic protein, bruchilot (brp), expressed from the endogenous promoter through recombination in flies of genotype UAS-tdTomato, brp > stop > GFP; MZ19-Gal4/UAS-FLP Recombinase. Presynaptic sites are visible in the antennal lobe glomeruli, mushroom body calyx and lateral horn.

(D and E) (D) Peak sytGCaMP fluorescence evoked by DA1 glomerular stimulation with acetylcholine and (E) basal fluorescence of sytGCaMP expressed in MZ19+ neurons (inset shows magnified boutons in calyx) indicating presynaptic localization that closely resembles the presynaptic sites identified by brp-GFP labeling in (B). Note the absence of sytGCaMP labeling on the shaft of PN axons that lack presynaptic sites. Green scales represent fluorescence intensity (A.U.) in same units for D-E.

(F) Comparison of soluble GCaMP6s and sytGCaMP response in KCs to minimal stimulation through acetylcholine iontophoresis into the mushroom body calyx. Note the individual presynaptic puncta clearly defined in the sytGCaMP signal compared to the more continuous GCaMP6s signal along the KC axons in the pedunculus.

(G) Immunostaining of larval NMJ with sytGCaMP expressed in motorneurons using VGlut-Gal4. α-GFP staining (green) shows co-localization of sytGCaMP with presynaptic cysteine string protein (CSP, left, red) and active zone protein bruchpilot (BRP, right, red). α−HRP staining (blue) labels motorneurons and highlights axon shaft.

(H) Expression of sytGCaMP under R16A06-Gal4 shows homogeneous and specific labeling of γ KCs by this driver line (left). All KCs express DsRed and allow us to define the different mushroom body lobes as indicated (right). Image was taken in a brain explant.

(I) Iontophoresis of acetylcholine into the mushroom body calyx was titrated to excite a single KC, as revealed by a sole activated process running through the pedunculus, and sytGCaMP response along the axon was captured by volumetric imaging. Note that in a brain explant, we observe a relatively uniform sytGCaMP signal at individual presynaptic sites along the entire length of the KC axon. Inset of the lobe is the same image used in Figure 1E.

(J) Co-expression of tdTomato and synaptotagmin-GFP in a subset of γ KCs under VT043657-Gal4 shows the distribution of presynaptic sites along the entire length of a KC axon. Dashed line outlines the γ lobe.

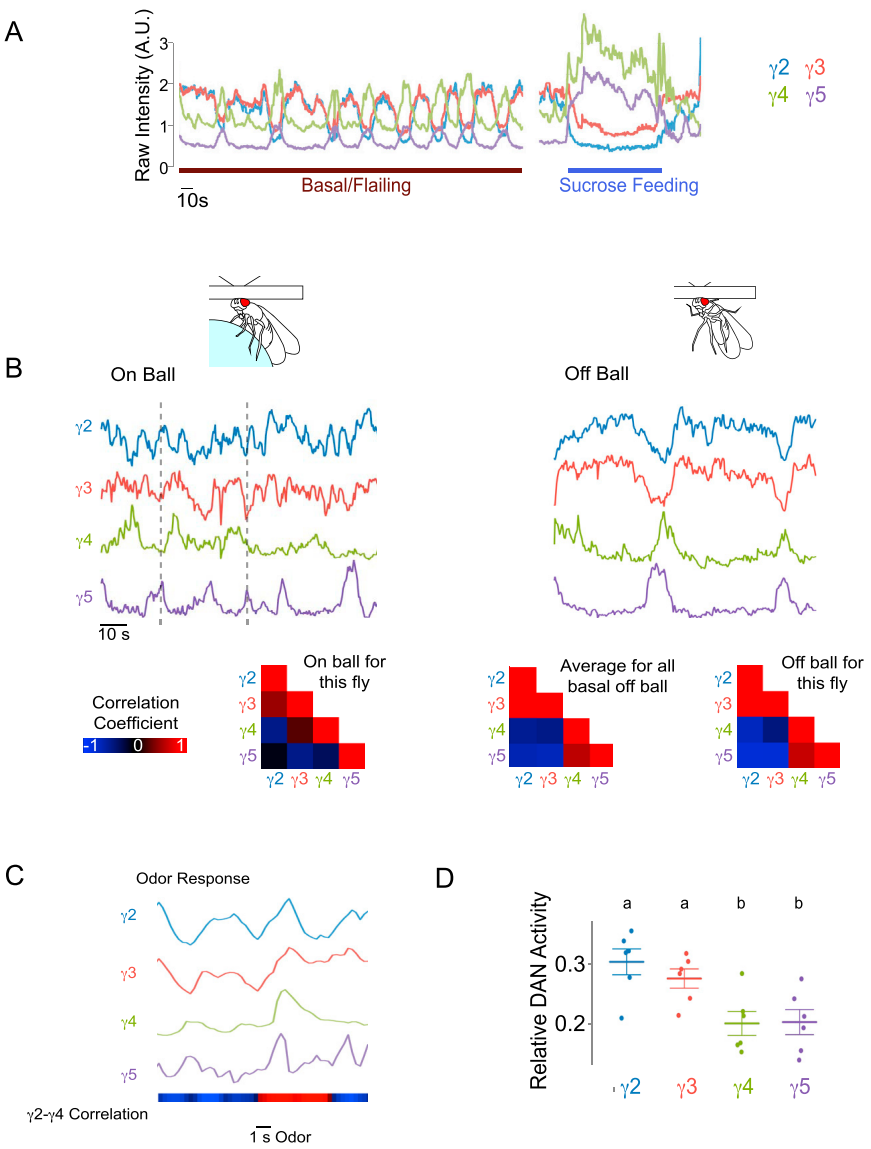

Figure S2. DAN Network Activity Reflects External Sensory Cues and Internal Behavioral State, Related to Figure 2

(A) Representative raw fluorescence traces of γ lobe DANs expressing sytGCaMP in the same fly without any external stimulus (left) and in response to sugar ingestion (right) show that sugar-induced responses of DANs are qualitatively similar, but quantitatively greater than baseline, motor correlated activity. Average sugar-induced responses were 2.2 (±0.35)-fold greater in the γ4 DAN and 4.8 (±0.8)-fold greater in the γ5 DAN compared to the amplitude of spontaneous fluctuations in the same flies (n = 9).

(B) Normalized basal intensity traces of γ lobe DANs expressing sytGCaMP for the same fly when walking on a freely rotating ball (top left) and when taken off of the ball and transitioning between quiescence and flailing behavioral states (top right). The correlations between all compartments are altered in these different behavioral contexts. Note for example that activity in γ3 and γ4 DANs, generally anti-correlated when the fly is dangling, become transiently correlated when the fly walks on a ball. Tethered, dangling flies exhibit a very consistent pattern of DAN correlations (compare individual and average for all flies, n = 12 traces in 6 flies, bottom), in accord with the notion that it underlies the consistent modulation of mushroom body processing we observe.

(C) Odor stimuli evoke responses in the DANs that alter basal correlations between dopaminergic compartments in a tethered animal. Representative traces of DANs show that odor (here isobutyl acetate) evokes increases in DANs of all 4 compartments, resulting in altered correlations between them. Note for example that odor evokes an increase in the correlation between γ2 and γ4 DANs, which basally are strictly anticorrelated in a tethered and dangling animal (bottom, correlation trace is running correlation of ten- imaging frames aligned to center frame. Correlation scale same as in (B)).

(D) Integrated normalized basal DAN activity in each compartment (n = 6 flies). Normalized intensities for each compartment were summed over entire recordings and each data point represents the sum for that compartment over the total sum for all four compartments in that fly.

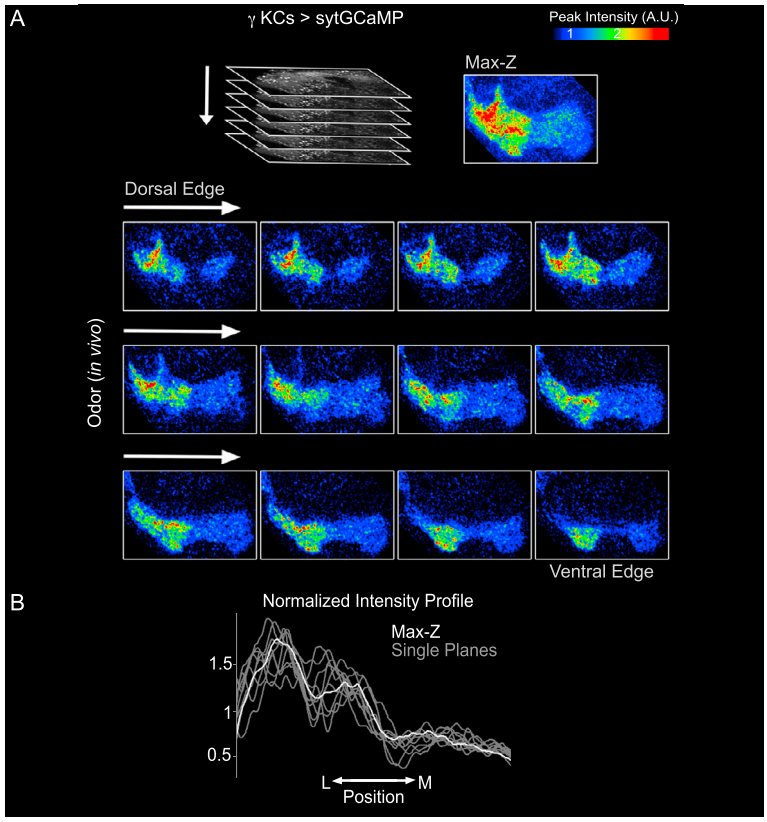

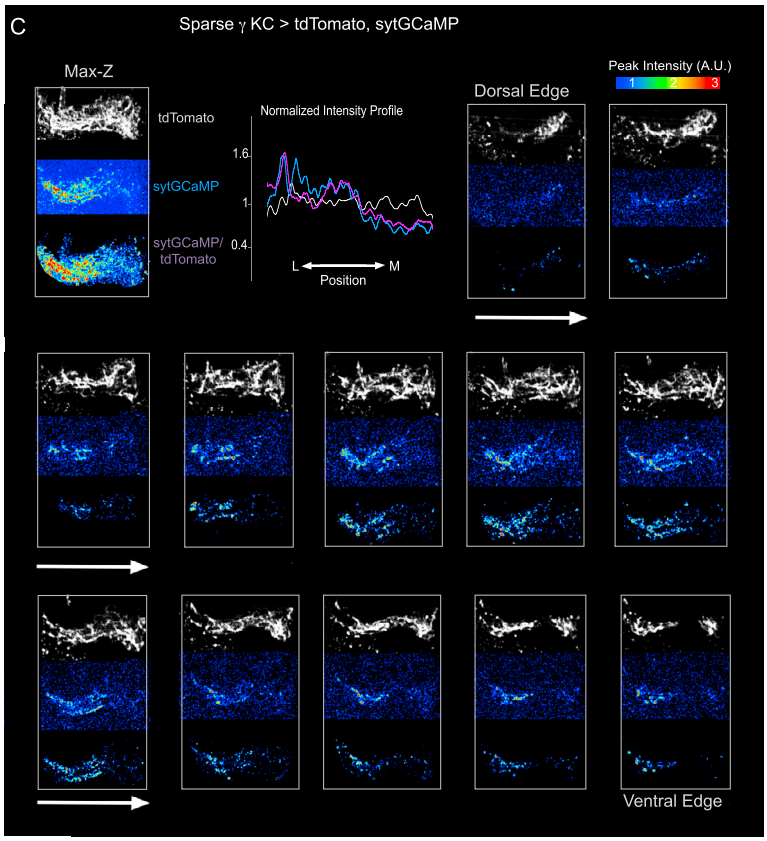

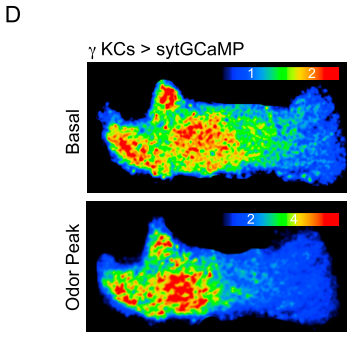

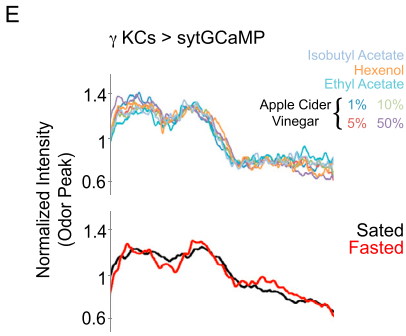

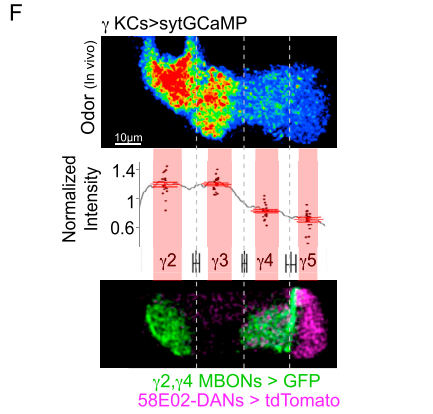

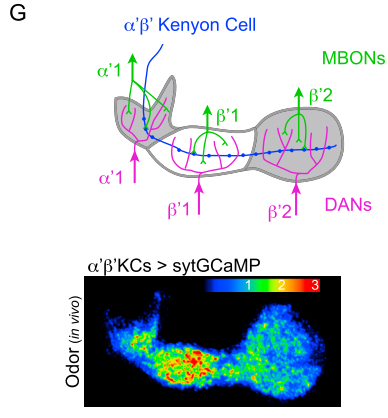

(legend on next page)

Figure S3. Rapid In Vivo Volumetric Imaging of γ Lobe Reveals Compartmentalized Presynaptic Ca^{2+} Distribution, Related to Figure 4

(A) Volumetric 2-photon resonant scanning imaging of γ KCs expressing sytGCaMP under R16A06-Gal4 in response to an odor stimulus. Schematic of imaging strategy (top-left inset). At each time point, data was collected at 12-18 Z-planes encompassing the entire γ lobe. Peak fluorescence of the 12 individual Z-planes and maximum Z projection (top-right) of the example shown in Figures 4A–4C. Compartmental differences in Ca^{2+} distribution are apparent in every imaging plane and the maximum-Z projection.

(B) Normalized intensity profile plot of sytGCaMP fluorescence along the length of the lobe for each imaging plane (gray) and of the maximum-Z projection (white) for the representative images shown in (A) indicate that every imaging plane displays a very similar Ca^{2+} distribution. (Only the 9 planes in which the entire length of the lobe is visible are included.)

(C) Volumetric imaging of sparsely labeled γ KCs co-expressing sytGCaMP and tdTomato confirms compartmentalized presynaptic Ca^{2+} differences along single KC axons that traverse the full length of the lobe. Representative images for the same sample shown in Figure 4F with tdTomato used to anatomically label axons (grayscale, top of each image), peak odor-evoked sytGCaMP fluorescence (heatmap, middle of each image) and peak sytGCaMP fluorescence normalized by tdTomato signal (see Supplemental Experimental Procedures) within each pixel (heatmap, bottom of each image). Maximum intensity Z projection (top-left), normalized intensity profiles (top-center) and each of the 12 optical planes from dorsal to ventral edge. Note that while the td-Tomato signal is uniform along the length of the lobe, the sytGCaMP signal is asymmetric and resembles the modular pattern apparent when imaging the total γ KC population. Odors used were isobutyl acetate in (A-B) and benzaldehyde in (C). However, a similar distribution of presynaptic Ca^{2+} was seen for all odor stimuli, see (E).

(D) Compartmentalized KC Ca^{2+} is also apparent in the basal state (top), prior to odor stimulation but becomes more apparent in odor-evoked responses (bottom). Note the heatmaps represent different intensity scales and there is a significant increase in sytGCaMP fluorescence evoked by an odor stimulus.

(E) The distribution of presynaptic Ca^{2+} along KCs was independent of odorant identity or satiety state. Normalized intensity profiles of peak fluorescence shown for isobutyl acetate, trans-3-hexen-1-ol, ethyl acetate, and apple cider vinegar at a range of concentrations (top, n = 4). Average normalized intensity profile of odor-evoked γ KC sytGCaMP fluorescence in sated flies (black, n = 21) and in flies that were food-deprived for 20-26 hr (red, n = 9) reveals no apparent difference in presynaptic Ca^{2+} distribution along the γ lobe (bottom).

(F) Registration strategy used to define compartmental borders. Fluorescent reporters were expressed in MBONs and DANs (bottom, n = 10, 1 representative example is shown) and labeling by extrinsic neuron innervation was used to define the average position of compartmental borders along the longitudinal axis of the γ lobe. The average border positions between compartments are indicated by dashed vertical lines. The SEM of the border positions are indicated between compartment names. To generate an average value of sytGCaMP intensity for each compartment (termed the compartment average in Figures 4 and 5) the intensity values for the center 50% of each compartment were averaged (red area, see experimental procedures for details). The representative image from Figure 4C is shown on top with the dot/box plot from Figure 4C below.

(G) Schematic of compartmentalized anatomic organization in the α' and β' lobes (top). Odor-evoked presynaptic Ca^{2+} signal in α'β' KCs visualized by expressing sytGCaMP under the R35B12-Gal4 driver (bottom) reveals compartmentalized signals similar to those observed in γ KCs. Image is a maximum intensity projection of peak odor-evoked fluorescence from volumetric imaging of the lobe.

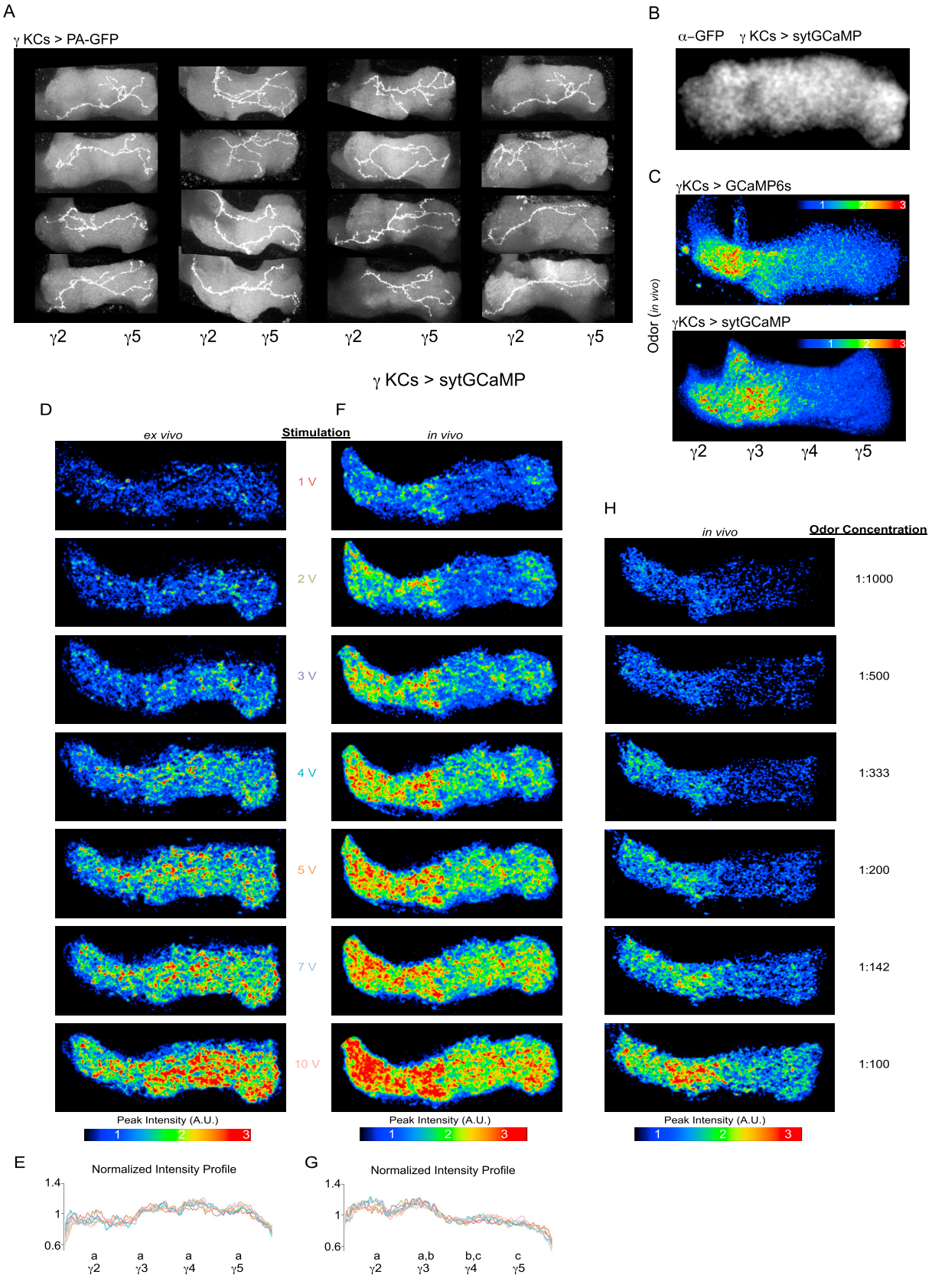

(legend on next page)

Figure S4. Modular Ca^{2+} Signals in γ KCs Reflect In Vivo Functional Modulation, Related to Figure 4

(A) Single KC labeling by PA-GFP expressed under the MB247 promoter demonstrates that γ KCs (n = 82, 16 shown) project their axons across the entire lobe, traversing all compartments.

(B) Immunolabeling of sytGCaMP expressed in γ KCs under the R16A06-Gal4 promoter with α-GFP staining reveals an equivalent distribution throughout the compartments of the lobe.

(C) Representative images comparing peak odor-evoked compartmentalized Ca^{2+} signal along the γ lobe in KCs expressing either soluble GCaMP6s or sytGCaMP. The asymmetric Ca^{2+} distribution is apparent in both cases but compartmental boundaries are more apparent with the synaptic resolution afforded by sytGCaMP. The approximate position of γ lobe compartments is indicated below.

(D) Representative images of peak sytGCaMP signal in γ KCs in response to direct stimulation of KCs by iontophoresis of acetylcholine on their dendrites in the mushroom body calyx in a brain explant. A range of iontophoretic voltages was used, as indicated.

(E) Normalized intensity profiles for experiment shown in (D). The color of the line in the profile plot indicates the iontophoretic voltage used as shown in (D). Each trace is the average of two stimulations at the indicated voltage for n = 6 mushroom bodies. Statistical analysis done using values averaged from traces at all voltages used. Values marked with different lowercase letters represent significant differences with $p < 0.05$ by t test with correction for multiple comparisons.

(F) Representative images for same stimulation protocol as in (D) in a tethered fly in vivo.

(G) Same as (E), but for in vivo data in (F), n = 6 mushroom bodies.

(H) Peak odor-evoked intensity in a living fly across a range of odor concentrations (isobutyl acetate).

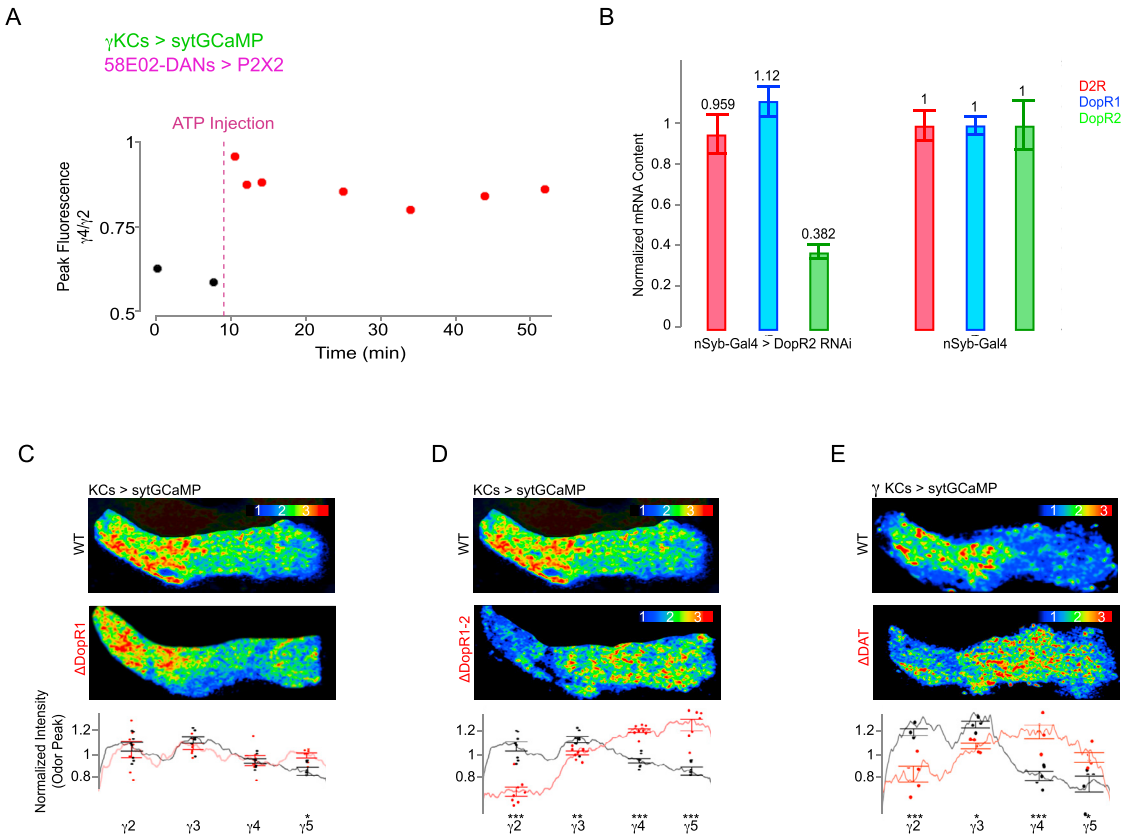

Figure S5. Dopaminergic Signaling Modulates the Presynaptic Ca^{2+} Distribution along KC Axons, Related to Figure 5

(A) Representative time course for experiment shown in Figure 5B shows that transient DAN-activation using $P2X_2$ (indicated by dashed line) induces a persistent shift in the pattern of odor-evoked presynaptic Ca^{2+} along KC axons. The ratio of the peak odor-evoked sytGCaMP signal for KC axon segments in the γ4 and γ2 compartments is plotted over the course of an experiment.

(B) Whole brain mRNA transcript levels quantified by RT-PCR for the indicated dopamine receptors in animals expressing DopR2-RNAi pan-neuronally using the synaptobrevin promoter (left) relative to transcript levels in Gal4 driver only control (right).

(C) Representative odor-evoked sytGCaMP fluorescence in WT and DopR1 mutant flies (top). Intensity profiles (bottom) for WT (black, n = 8 mushroom bodies) and DopR1 (red, n = 7 mushroom bodies) flies show that DopR1 profiles are somewhat more uniform, with a slight but significant difference in Ca^{2+} distribution apparent in γ5.

(D) As in (B) but for DopR1, DopR2 double mutant, n = 8 mushroom bodies.

(E) As in (B) but for the dopamine reuptake transporter (DAT) mutant, n = 5.

Significant differences in relative compartment intensity compared to WT indicated by *p < 0.05, **p < 0.005, ***p < 0.0005.

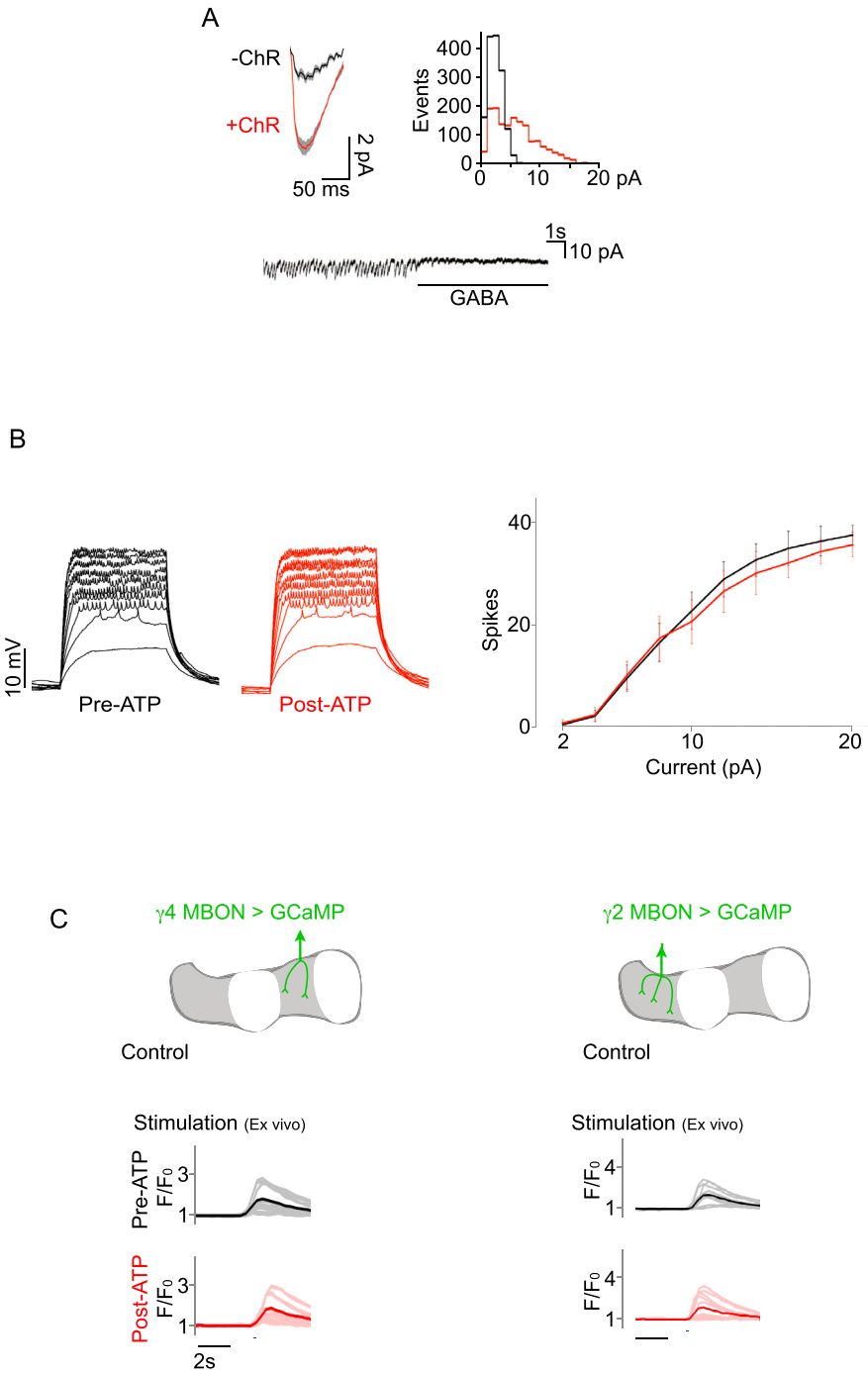

Figure S6. DANs Modulate KC-MBON Synaptic Transmission, Related to Figure 6

(A) Mean γ4 MBON spontaneous EPSC profiles (top-left) and histogram of EPSC amplitudes (top-right) with (red) and without (black) ReaChR expressed in R58E02+ DANs (n = 5 flies ReaChR, n = 6 flies control, $p < 0.0005$). GABA injection into the KC dendrites on the mushroom body calyx suppresses spontaneous EPSCs measured in the γ4 MBON (bottom).

(B) Representative KC spike trains evoked by 2 pA current steps in KC current clamp recordings before and after activation of 58E02+ DANs through $P2X_2$ (left). Mean (+/− SEM) number of spikes evoked by current injection in KC current clamp recordings show no apparent change in KC properties following DAN activation (right, n = 6 flies, $p > 0.6$).

(C) Control data for experiments shown in Figure 6B-C. Injection of ATP had no effect on MBON responses to direct KC stimulation in control animals that lacked $P2X_2$ expression in DANs (γ4 MBON on left, n = 6 flies, $p > 0.3$, γ2 MBON on right, n = 6 flies, $p > 0.6$).

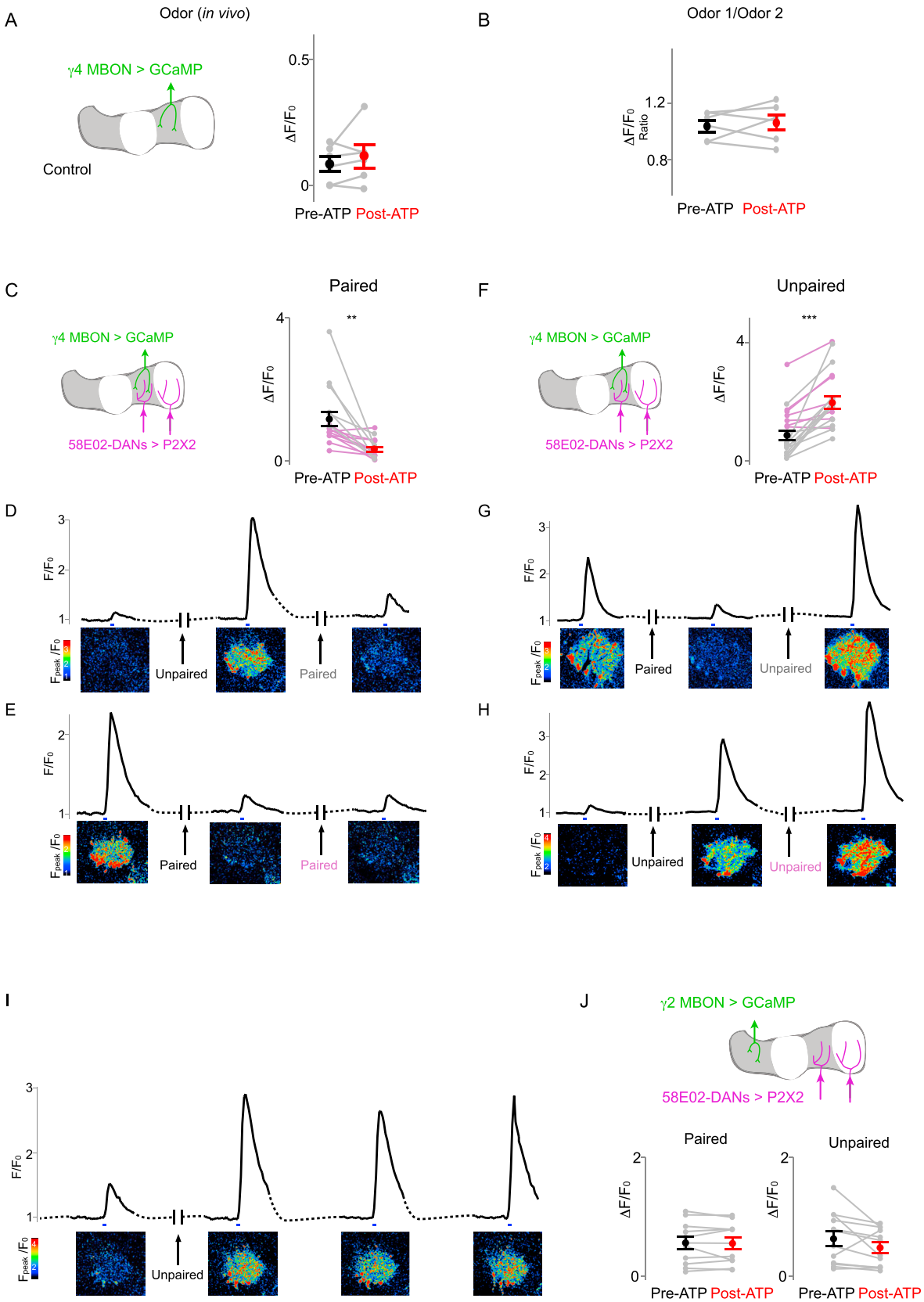

(legend on next page)

Figure S7. Bidirectional Modulation of KC-MBON Signaling, Related to Figure 7

(A) Control data for experiments shown in Figure 7D. Injection of ATP had no effect on γ4 MBON olfactory responses in control animals that lacked $P2X_2$ expression in DANs (n = 6 flies, p > 0.16).

(B) The potentiation of MBON olfactory responses by unpaired DAN activation is independent of odor identity. The responses of the γ4 MBON to hexanol and isobutyl acetate were equivalently enhanced after activation of 58E02+ DANs, such that the ratio of the responses remained unchanged (n = 6 flies, p > 0.6). This is in contrast to the odor-specific depression evident using these same odors, after pairing one odor with DAN stimulation as shown in Figure 7J.

(C) Paired KC-DAN stimulation depresses KC-MBON signaling independent of the previous synaptic state. Data from Figure 7I is replotted (gray), in which the effect of paired KC and DAN stimulation on MBON responses was examined from an initially potentiated synaptic state (as in D) or from a previously depressed state (pink, as in E).

(D) Representative time course of γ4 MBON GCaMP fluorescence in response to direct KC stimulation in which 58E02+ DANs expressing $P2X_2$ were alternately activated in the absence of KC stimulation (unpaired), or synchronously with KC stimulation (paired). Paired KC-DAN activation resulted in depression of MBON responses that had been previously potentiated (gray lines in C). Time courses (top, same traces shown in Figure 7H) and heatmaps (bottom) of the γ4 MBON response with stimulation protocol indicated between recordings. Blue lines indicate KC stimulation. Dashed lines in all panels indicate a delay of > 45 s.

(E) As in D, showing that paired DAN-KC activation further depresses or has no effect on MBON responses if they had been previously depressed (pink lines in C).

(F) Unpaired KC-DAN stimulation potentiates KC-MBON signaling independent of the previous synaptic state. Unpaired data from Figure 7I is replotted (gray), in which the effect of unpaired DAN activation on MBON responses was examined from an initially depressed synaptic state (as in G) or from a potentiated state (pink, as in H).

(G) As in D, showing that unpaired KC-DAN activation potentiates the MBON response that had been previously depressed (gray lines in F).

(H) As in D, showing that unpaired KC-DAN activation further potentiates MBONs had been previously potentiated (pink lines in F).

(I) As in D-H, but for a series of KC stimulations in which there was only a single, unpaired activation of 58E02+ DANs, showing that γ4 MBON responses are stable over successive recordings after potentiation by dopamine.

(J) Stimulation of 58E02+ DANs had no effect on γ2 MBON responses to KC stimulation whether KC-DAN activation was synchronous (paired) or DANs were activated independently of KC stimulation (unpaired).

Cell

Supplemental Information

Coordinated and Compartmentalized Neuromodulation Shapes Sensory Processing in *Drosophila*

Raphael Cohn, Ianessa Morantte, and Vanessa Ruta

Supplemental Experimental Procedures

Generation of sytGCaMP Transgenic Flies

The coding sequence for GCaMP6s (Chen et al., 2013) (Addgene Plasmid #40753) was appended to the *Drosophila* synaptotagmin 1 coding sequence (DGRC Stock #4839) with an intervening 3xGS linker by PCR and Gibson Assembly (Gibson, 2009). The resulting product (sytGCaMP) was ligated into pJFRC-10xUAS (Addgene Plasmid #36432) and pJFRC-LexAOP (Addgene Plasmid #26224) and used to generate transgenic flies by PhiC31-based integration into attp40, attp5 and VK00005 by Bestgene Inc. Additional transgenics were generated in which GCaMP6s was tethered to synaptogyrin (DGRC Stock #17821) but preliminary expression studies in projection neurons (as in Figure S1) revealed inferior presynaptic localization with fluorescence along the shaft of axons lacking presynaptic sites (data not shown).

Fly Strains

Flies were maintained on conventional cornmeal-agar-molasses medium at 23-25°C and 60-70% relative humidity, under a 12 hr light: 12 hr dark cycle.

Strains and sources:

VT026001-Gal4, VT043657-Gal4, VT203149-Gal4 (Vienna Drosophila Resource Center (VDRC); https://braingazer.org/brainbaseweb); *R25D01-Gal4, R93B07-Gal4, R66C08-Gal4, R16A06-Gal4, R35B12-Gal4, R53C03-LexA, R25D01-LexA, R14C08-LexA, R58E02-Gal4, R58E02-LexA* (Jenett et al., 2012; http://flweb.janelia.org/cgi-bin/flew.cgi)*, UAS-GCaMP6s, UAS-tdTomato, LexAOP-tdTomato, LexAOP-ReaChR* (Inagaki et al., 2014)*, MZ19-Gal4* (Ito et al., 1998), *VGlut-Gal4*, *UAS-DopR2-RNAi* (TRiP.HMC02893, generated by the TRiP at Harvard Medical School (NIH/NIGMS R01-GM084947)) *(Bloomington Drosophila Stock Center); MB247-DsRed* (Riemensperger et al., 2005) (gift from Andre Fiala, University of Göttingen); *MB247-LexA* (Pitman et al., 2011) (gift from Scott Waddell, University of Oxford); *LexAOP-P2X*$_2$ (Yao et al., 2012) (gift from Orie T. Shafer, University of Michigan); *OK107-Gal4* (Connolly et al., 1996); *TH-Gal4* (Friggi-Grelin et al., 2003); *DDC-Gal4* (Li et al., 2000); *Tub>Gal80>* (Gordon and Scott, 2009) (gift from Kristin Scott, University of California, Berkeley); *fmn* dDAT mutant (Kume et al., 2005); *DopR1*^{attP}, *DopR2*^{attP}(Keleman et al., 2012), *DopR1*^{attP}*-DopR2*^{attP} Double Mutant (Gift from Daisuke Hattori); *UAS-C3PA-GFP*, *LexAOP-SPAGFP-T2A-SPAGFP* (Ruta et al., 2010).; *UAS-FLP*, *brp>STOP>GFP* (Chen et al., 2014) (gift from Larry Zipursky, University of California, Los Angeles).

Detailed fly genotypes used by figure (with neuronal expression description):

Figures 1B and S4A:
LexAOP-SPA-T2A-SPA;MB247(KCs)-LexA, LexAOP-SPAGFP
Figures 1C, 7A-7C and 7F:
UAS-GCaMP6s;VT026001(γ4-MBON)-Gal4,UAS-GCaMP6s/R25D01(γ2-MBON)-Gal4
UAS-GCaMP6s/UAS-GCaMP6s;R93B07(γ3-MBON)-Gal4/R66C08(γ5-MBON)-Gal4
Figure 1D:
UAS-C3PA-GFP/UAS-C3PA-GFP;TH(DAN subset)-Gal4, DDC(DAN subset)-Gal4/UAS-C3PA-GFP
Figures 1E, 4A-4D, 5A, 5E, S1I, S3A-S3B, S3D-S3F, S4B-S4H and S5E:
UAS-sytGCaMP;R16A06(γ KCs)-Gal4
Figures 2 and S2 :
UAS-sytGCaMP, MB247(KCs)-DsRed;TH(DAN subset)-Gal4, DDC(DAN subset)-Gal4
Figure 3A:
UAS-sytGCaMP, MB247(KCs)-DsRed/R58E02(γ4-5 DANs)-LexA;TH(DAN subset)-Gal4, DDC(DAN subset)-Gal4/LexAOP-P2X2
Figure 3B:
UAS-sytGCaMP, MB247(KCs)-DsRed/R25D01(γ2 MBON)-LexA;TH(DAN subset)-Gal4, DDC(DAN subset)-Gal4/LexAOP-P2X2
Figure 3C:
UAS-sytGCaMP, MB247(KCs)-DsRed/R93B07(γ3 MBON)-LexA;TH(DAN subset)-Gal4, DDC(DAN subset)-Gal4/LexAOP-P2X2
Figure 3D:

UAS-sytGCaMP, MB247(KCs)-DsRed/R53C03(γ4 MBON)-LexA;TH(DAN subset)-Gal4, DDC(DAN subset)-Gal4/LexAOP-P2X2
Figure 3E:
UAS-sytGCaMP, MB247(KCs)-DsRed/R14C08-LexA(γ5 MBON);TH(DAN subset)-Gal4, DDC(DAN subset)-Gal4/LexAOP-P2X2
Figure 4E:
UAS-sytGCaMP/R58E02(γ4-5 DANs)-LexA;R16A06(γ KCs)-Gal4/LexAOP-tdTomato
Figures 4F and S3C:
hsFLP;UAS-sytGCaMP/UAS-tdTomato;R16A06(γ KCs)-Gal4/Tub>Gal80>
Figures 5B and S5A:
UAS-sytGCaMP/R58E02(γ4-5 DANs)-LexA;R16A06(γ KCs)-Gal4/LexAOP-P2X2
Figure 5C:
UAS-sytGCaMP;R16A06(γ KCs)-Gal4/(LexAOP-P2X2)
Figures 5D:
UAS-sytGCaMP;DopR2^{attP}/DopR2^{attP};OK107(KCs)-Gal4
UAS-sytGCaMP;;OK107(KCs)-Gal4
Figure 5E:
UAS-sytGCaMP/UAS-DopR2-RNAi;16A06(γ KCs)-Gal4
Figures 6A-6B, 7D, 7G-J and S7B-I:
UAS-GCaMP6s/R58E02(γ4-5 DANs)-LexA;VT026001(γ4-MBON)-Gal4,UAS-GCaMP6s/LexAOP-P2X2
Figure 6C:
R25D01(γ2 MBON)-LexA/UAS-P2X2;VT203149(γ2 DAN)-Gal4/LexAOP-GCaMP6s
Figures 6D, 7E, and S7J:
R58E02(γ4-5 DANs)-LexA/UAS-GCaMP6s;25D01(γ2 MBON)-Gal4/LexAOP-P2X2
Figure 6E:
R53C03(γ4 MBON)-LexA/UAS-P2X2;VT203149(γ2 DAN)-Gal4/LexAOP-GCaMP6s
Figure S1C:
MZ19(PN subset)-Gal4/UAS-tdTomato;UAS-FLP,brp>STOP>GFP
Figures S1D-S1E:
MZ19(PN subset)-Gal4/UAS-sytGCaMP;UAS-tdTomato
Figure S1F:
UAS-sytGCaMP;;OK107(KCs)-Gal4
UAS-GCaMP6s;;OK107(KCs)-Gal4
Figure S1G
VGlut(motorneurons)-Gal4;UAS-sytGCaMP;
Figure S1H:
MB247(KCs)-DsRed/UAS-sytGCaMP;R16A06(γ KCs)-Gal4
Figure S1J:
UAS-tdTomato, UAS-sytGFP;VT043657-Gal4
Figure S3F:
R58E02(γ4-5 DANs)-LexA, LexAOP-tdTomato;VT026001(γ4-MBON)-Gal4,UAS-GFP GCaMP6s/R25D01(γ2-MBON)-Gal4
Figure S3G:
UAS-sytGCaMP;R35B12(α'β' KCs)-Gal4
Figure S4C:
UAS-GCaMP6s;R16A06*(γ KCs)*-Gal4
Figure S5B:
nSyb(neuronal)-Gal4
nSyb(neuronal)-Gal4/UAS-DopR2-RNAi
Figure S5C:
UAS-sytGCaMP;DopR1^{attP}/DopR1^{attP};OK107(KCs)-Gal4
Figure S5D:
UAS-sytGCaMP;DopR1^{attP}, DopR2^{attP}/ DopR1^{attP},DopR2^{attP};OK107(KCs)-Gal4
Figure S5E:
dDAT mutant/dDAT mutant;R16A06(γ KCs)-Gal4/UAS-sytGCaMP
Figure S6A:

UAS-GCaMP6s/R58E02(γ4-5 DANs)-LexA;VT026001(γ4-MBON)-Gal4/LexAOP-ReaChR
Figure S6B:
UAS-GFP/R58E02(γ4-5 DANs)-LexA;R16A06(γ KCs)-Gal4/LexAOP-P2X2
Figure S6C:
UAS-GCaMP6s;VT026001(γ4-MBON)-Gal4,UAS-GCaMP6s/(LexAOP-P2X2)
R25D01(γ2 MBON)-LexA/(UAS-P2X2);LexAOP-GCaMP6s

Sparse Labeling
Sparse labeling of γ KCs for functional imaging (Figures 4F and S3C) was achieved by stochastic excision of ubiquitous Gal80 repression through expression of FLP-recombinase under the heat-shock promoter as described (Wu and Luo, 2006). Briefly, flies with the genotype: hsFLP;UAS-sytGCaMP/UAS-tdTomato;R16A06*(γ KCs)*-Gal4/Tub>Gal80>, were incubated at 21°C to reduce spontaneous FLP-recombinase activation and transferred into new vials every 1-2 days. During the late pupal stage the vials were heatshocked by immersion in a 37°C water bath for 10-30 minutes and then returned to incubation at 21°C until dissection.

Imaging
All functional imaging experiments were performed on an Ultima two-photon laser scanning microscope (Bruker Nanosystems) equipped with galvanometers driving a Chameleon Ultra II Ti:Sapphire laser. Emitted fluorescence was detected with either photomultiplier-tube or GaAsP photodiode (Hamamatsu) detectors. Images were acquired with an Olympus 60×, 0.9 numerical aperture objective at 512 pixels × 512 pixels resolution. For fast-scanning volumetric imaging *in vivo*, the laser was directed through an 8kHz resonant scanning galvonometer and the objective was controlled by a piezo-electric Z-focus. Z-planes were defined in order to encompass the entire volume of the γ lobe. 12-18 planes were recorded, spaced ~2 μm apart and the entire volume was imaged at a rate of ~1.5Hz.

Photolabeling of neurons
To photolabel DANs innervating specific γ lobe compartments (Figure 1C) we expressed C3PA-GFP in most DANS driven by the combination of TH-Gal4 and DDC-Gal4. To label individual γ KCs (Figures 1B and S4A) we expressed SPA-GFP in all KCs driven by MB247-LexA. We targeted specific γ lobe compartments (for DAN labeling) or individual KC soma (for single KC labeling) using 925 nm laser illumination, a wavelength that does not cause significant photoconversion. To photolabel neurons, we defined an ROI in PrairieView Software in a single Z-plane and exposed the target area to 710 nm light (~10-30 mW at the back aperture of the objective) 10-15 times. After diffusion of the photoconverted fluorophores throughout the targeted neurons for 10-30 minutes, we imaged at 925 nm using 1 μm steps.

Functional Imaging
For *ex vivo* experiments brains were dissected in external saline (108 mM NaCl, 5 mM KCl, 2 mM $CaCl_2$, 8.2 mM $MgCl_2$, 4 mM $NaHCO_3$, 1 mM NaH_2PO_4, 5 mM trehalose, 10 mM sucrose, 5 mM HEPES pH7.5, osmolarity adjusted to 275 mOsm), briefly treated with collagenase in external saline (2 mg $mL^{-1,}$ 30 sec), washed, and then pinned with fine tungsten wires to a thin Sylgard sheet (World Precision Instruments) in a 35 mm petri dish (Falcon) filled with saline. For *in vivo* imaging, flies were prepared as previously described (Murthy and Turner, 2013a; Ruta et al., 2010). Briefly, 2-5 day old flies were temporarily anaesthetized using CO_2 (for <30 s) and then tethered to a piece of tape covering a hole in the bottom of a modified 35 mm petri dish using a human hair placed across the cervical connectives. A small hole was cut into the tape, precisely above the head, to allow the top of the head capsule to extend above the plane of the tape. A dot of UV-curable glue (Loctite) was applied to the eyes to restrict head movement. The dish was then filled with external saline and the head capsule was opened by carefully cutting and folding back the flap of cuticle covering the dorsal portion of the head. Muscle 16 and obstructing trachea were removed with sharpened forceps. In ATP and acetylcholine injection experiments, the open head capsule was briefly bathed in collagenase (2 mg mL^{-1}, 30 sec) to weaken the perineural sheath. Care was taken to keep the antennae and antennal nerves intact. On rare occasions, flies showed no movement or odor responses and were discarded.

Volumetric imaging of single KC in a brain explant

To visualize Ca^{2+} influx throughout the axonal arbor of a single KC (Figures 1E and S1I) with high spatial resolution, the same voltage was used to repeatedly iontophoretically stimulate the calyx with acetylcholine as described below, allowing for equivalent activation of the neuron at each of 45 planes spaced ~1 μm apart. The representative image shown is the maximum Z-projection of the peak intensity response to stimulation for each imaging plane. In comparison to volumetric imaging by resonant scanning used *in vivo* (below), this strategy yielded better image quality due to greater temporal averaging at this slower scanning rate.

Odor stimulation

Odor stimulation was achieved by directing a continuous stream (400-500 mL/min) of clean air through a 2 mm diameter teflon tube directed at the fly's antenna (carrier stream). 5-10% of the total airstream was diverted through the headspace of a 10 mL glass vial containing paraffin oil (odor stream). At a trigger, a custom-built solenoid valve controller system redirected the odor stream from a blank vial to a vial containing various odorants diluted in paraffin oil (Sigma) to a final volume of 1 mL. Final odorant dilutions were between 1:20-1:200, depending on the identity of the odorant. In experiments where odor concentration was varied (Figures S3E and S4H), the fraction of odor stream directed to the fly was adjusted to give final concentrations between 1:100 and 1:1000. Odorants used were isobutyl acetate (CAS #110-19-0), trans-3-hexen-1-ol (CAS #928-97-2), benzaldehyde (CAS #100-52-7), 3-octanol (CAS #589-98-0), methancyclohexanol (CAS #589-91-3) and Apple Cider Vinegar (Heinz). In a subset of experiments, a fraction of the olfactometer output air stream was redirected to a mini-PID (Aurora Scientific) in order to measure odorant waveforms and ensure the consistency of odor presentations across trials. Given that we observed no difference in the patterns of pre-synaptic Ca^{2+} along KC axons or MBON responses to different odorants, we averaged responses across odors to generate the normalized odor-evoked sytGCaMP profile in Figures 4 and 5 and to generate MBON response profiles in Figure 7B and 7D-7F.

Activation of $P2X_2$-expressing Neurons by ATP Injection

To activate DANs or MBONs expressing $P2X_2$ (Figures 3, 5B-C, 6, 7D-E, 7G-J, S5A, S6B-C and S7) a glass stimulating electrode, pulled to a resistance of 7-10 MΩ, was filled with 2 mM ATP in external saline. Stimulating electrodes were positioned dorsal to the mushroom body's medial lobes, in the superior medial protocerebrum, at the site of rich γ4 and γ5 DAN dendritic and MBON axonal innervation. In some experiments tdTomato was co-expressed in 58E02+ DANs to serve as an anatomic guide. The stimulating electrode was coated with BSA-conjugated Texas Red Dye (Life Technologies) in order to visualize electrode position (Ishikawa et al., 2010). In experiments examining *in vivo* modulation of KC presynaptic Ca^{2+} (Figures 5B-C and S5A), ATP was injected in short bursts (~15 pulses) over the span of 2-3 minutes, with >1 minute between the pre-injection odor stimulus and the start of injection and >1 minute recovery period following injection before post-injection odor stimulus. For all other experiments involving ATP injection a single brief pulse of positive pressure was applied manually or using a custom-built pressure injector. Protocol for ATP stimulation in other experiments described below.

Calycal and Glomerular Stimulation

Glass stimulating electrodes were pulled to a resistance of 7–10 MΩ and then filled with 10 mM acetylcholine (Sigma) in external saline. Stimulating electrodes were positioned into the mushroom body calyx (Figures 1E, 4D, 6, 7C, 7H-I, S1F, S1I, S4D-G, S6C and S7C-J) or the center of the DA1 glomerulus (Figure S1D) viewed under IR-DIC optics. Square voltage pulses (500 ms long, 0.1-10V for all imaging experiments, 0.1-2ms long, 10-100V for electrophysiology in Figure 6A) generated by a stimulator (Grass Technologies) were used to excite Kenyon cell or antennal lobe projection neuron dendrites. To account for variation in electrode tip and positioning, the iontophoretic voltage was titrated to evoke robust but non-saturating responses in the neurons being recorded. For Figures 1E, S1F and S1I, the iontophoretic voltage was titrated until 1-2 KCs were stimulated, as evident by a sole active process running through the pedunculus where KC axons are unbranched, fasciculated, and parallel. For Figures S4D-S4G, stimulation was performed twice at each voltage indicated between 1-10V.

Paired and Unpaired Stimulation Protocols

For 'paired' stimulation of DANs and KCs, KC stimulation and DAN activation via ATP injection were temporally paired as illustrated in Figure 7G. In experiments where KCs were directly activated (Figures 7H-I and S7C-J) KC stimulation was performed as described above for a duration of 500 ms, immediately followed by a 200 ms ATP injection via pressure injector as described above. For odor stimulation *in vivo* (Figure 7J), two odors (isobutyl acetate and hexanol) were each presented as described above at least 2 times with >45 seconds between exposure to establish stable baseline responses. One of the odors was then paired with a 200 ms pressure pulse of ATP beginning 500 ms after the start of the odor pulse. Each odor was used as the 'paired' odor in alternate experiments in order to control for any odor-specific effects. All DAN activation experiments were 'unpaired' unless noted. In 'unpaired' experiments, KC stimulation or odor presentation were performed >45 seconds before and after ATP injection in order to temporally separate DAN and KC activation.

Tethered Fly Behavior

Recording Fly Motor Activity

To simultaneously record the fly's motor activity during imaging (Figures 2B, 2D-2E, and S2) a Point Grey Firefly Camera with Infinity Lens (94 mm focal length) was focused on the fly, which was illuminated by infrared LED lights. Video was captured at 30 frames per second. Fly motion traces were extracted using a custom Matlab script that measures average absolute difference in pixel intensities between each frame and the preceding frame. Manual inspection of this automated analysis confirmed that it accurately registers the difference between the two behavioral states (flailing and quiescence) we observed in the tethered fly. Laser-scanning onsets and offsets, visible in the video recordings due to laser illumination through the head-capsule were used to align videos with imaging data. In light of the demonstrated correlation between DAN activity state and fly locomotion, we note that all other imaging experiments were performed without regard for the fly's behavioral state, which was presumably a comparable alternating pattern of flailing and pausing.

Sugar feeding (Figures 2B, 5A, 7F and S2A)

1-3 day old flies were fasted for 20-26 hours by transferring to an empty vial containing only a damp Kim-wipe. Flies were tethered for imaging as described above and positioned on the microscope. After recording baseline neural responses, a small wick of Kim-wipe fibers soaked in 0.2-1 M sucrose solution was positioned near the fly's proboscis using a motorized micromanipulator (Scientifica). The wick was touched to the proboscis to initiate feeding. Blue food coloring was added to the sucrose solution and fly abdomens were inspected after each experiment to confirm sucrose ingestion. Data for flies that had not consumed the sucrose solution were discarded. We observed no apparent difference in evoked changes in KC activity (Figure 5A) depending on sucrose concentration so data from different stimulations were pooled. For DAN and MBON imaging (Figures 2B and 7F) 0.2 M sucrose solution was uniformly used.

Electric Shock (Figure 2C)

The *in vivo* dissection dish described above was modified so that two steel threaded studs (McMaster-Carr) could be precisely positioned to make contact with either side of the fly's abdomen during tethering. The ends of the steel electrode leads were connected to a stimulator (Grass Technologies), which was used to apply a 500 ms pulse of 60-150V, comparable to the electrical shock parameters used in classical olfactory conditioning paradigms (Tempel et al., 1983; Tully and Quinn, 1985). Current flow through the circuit was monitored by an oscilloscope and the stimulating voltage was adjusted to maintain approximately equivalent current flow across trials to compensate for buildup of resistance following shocking.

Simulated walking (Figure S2B)

A small foam ball (~1 mm diameter, Matsubara Sangyo Co.) (Kohatsu et al., 2011) was positioned within the fly's grasp to allow the fly to 'walk' on the ball during imaging. Placement was adjusted to ensure free range of motion over 360°.

Image processing and Data Analysis

All image processing was done using FIJI/ImageJ (NIH). Further analysis was performed using custom scripts in ImageJ, Microsoft Excel, Matlab and R. When necessary, to correct for motion during *in vivo* imaging, recordings were stabilized using the StackReg ImageJ plugin. When neurons were co-labeled with

tdTomato, the MultiStackReg ImageJ plugin was used to stabilize the red channel and the transformations generated were applied to the green functional imaging channel. Images were smoothed with a Gaussian filter (s of 1-2 pixels). Areas outside of the γ lobes were partially masked in representative images for clarity as indicated.

Intensity profile plots (Figures 4C-D, 5, S3B-C, S3E-F, S4E, S4G and S5C-E)
The frame containing the peak fluorescence (see below) from an odor stimulus was manually rotated so that the longitudinal axis of the γ lobe lay along the x-axis, with the lateral-most edge at x=0. Regions outside of the γ lobe, easily distinguishable from the dense KC labeling within the lobe, were manually masked in each image. To generate the intensity profile across the lobe, we averaged the intensity of all pixels along the y-axis, for each point x along the horizontal axis of the lobe. To account for variations in imaging orientation, the resulting profiles were normalized to the same length (1000 'pixels') by linear interpolation. The average raw profile length was 315 pixels with a standard deviation of 19 pixels. The resulting 1000 'pixel' profile plots were smoothed by calculating a moving average of 30 'pixels' (3% of the total profile length). Each intensity profile was normalized to its mean intensity value in order to allow for comparison across animals and conditions. Similar results were obtained from normalizing to the maximum intensity value or median intensity value. For every data point, the plots of 2 odor-evoked profiles were averaged to correct for any motion artifacts. Because we observed no difference in the Ca^{2+} profiles evoked by different odorants (Figure S3E), we averaged data across odor stimuli. Initial experiments were carried out using the maximum intensity projection from volumetric imaging experiments. However, as we observed little variation in the intensity profile across imaging planes (Figure S3A-B), we combined data from experiments collected in traditional galvo scanning mode at single planes with maximum intensity Z-projections from resonant scanning volumetric data. When single planes were imaged, we chose planes that revealed the largest longitudinal portion of the lobe and contained γ2-γ5 compartments.

Quantification of neural activity using functional Ca^{2+} imaging is typically performed by normalizing the change in intensity by the pre-stimulus intensity ($\Delta F/F_0$). This normalization helps control for variations in reporter expression and imaging parameters so that comparisons can be made between different neurons or different experiments. In quantifying the modulation of KC synapses, however, we found this measure to be inappropriate. The asymmetric distribution of Ca^{2+} along KC axons is often apparent in the basal state (Figure S3D), prior to odor stimulation. Differences in synaptic Ca^{2+} along KCs are not present in the brain explant (Figures 4D and S4D-E) indicating that they reflect *in vivo* modulation rather than differences in sytGCaMP expression (Figure S4D). Therefore, normalizing odor-evoked responses by the basal fluorescence values would serve to mitigate the modulation we were seeking to quantify. Thus to quantify Ca^{2+} distribution along the γ lobe we used the peak intensity values.

To calculate the change in intensity profiles due to artificial (Figures 5B-5C) or physiological DAN activation from sugar feeding (Figure 5A), we subtracted the average normalized intensity profile measured prior to DAN activation from the average normalized intensity profile after activation in each fly. The resulting difference plot was averaged across flies.

Compartmental border determination:
To generate an average intensity value for each compartment of the γ lobe (Figures 4C, 5, S4E and S4G), we needed to accurately define compartmental borders. In order to define consistent compartmental borders, we used the strategy outlined in Figure S3F. Specifically, flies with fluorescently labeled DANs and/or MBONs (n=10 including TH-Gal4, DDC-Gal4>UAS-GCaMP6s; 58E02-LexA>LexAOP-tdTomato; 25D01-Gal4, VT026001-Gal4>UAS-GCaMP6s) were aligned and profiled as described above to generate the intensity profile plots for KCs. Regions of extrinsic neuron innervation in each compartment were used to generate average border positions, that divided the 1000 'pixels' along the x-axis. We defined the average γ2-3 border at pixel x=297, γ3-4 border at pixel x=560 and γ4-5 border at pixel x=821. The border positions were relatively consistent across animals but showed minor variability due to inevitable individual anatomic variation and differences in imaging orientation (see SEM depicted in Figure S3F). Therefore, to account for any potential uncertainty in the border assignment, we calculated the intensity value for each compartment by averaging pixels within the area comprising only the middle 50% of each compartment within the calculated borders. These values were used to calculate significance of

intercompartmental differences within individuals (Figures 4C-D, and S4D-G), changes within compartments due to DAN activity (Figures 5A-C and S5A) and differences between control profiles and dopamine signaling mutants or RNAi (Figures 5D-E and S5C-E).

For imaging of DANs and MBONs (Figures 2, 3, 6B-E, 7, S2, S6C and S7), ROIs were manually drawn based on the clear anatomic segregation of their innervation patterns in different compartments. For KC time-series traces (Figures 4C-D) ROIs were defined by compartmental border determination as described above. For single synapse time-series traces (Figure 4F), circular ROIs were manually drawn around individual synapses along the length of the lobe, identified by puncta labeled with sytGCaMP. In sparsely labeled KC axons co-expressing sytGCaMP and tdTomato, the tdTomato signal was first used to generate a mask in order to eliminate background signal due to low basal fluorescence outside of the labeled axons. The sytGCaMP odor responses were then divided by the tdTomato signal on a pixel-by-pixel basis. For $\Delta F/F_0$ calculations in DANs and MBONs the difference between the pre-stimulus value (average of 4-5 frames ending >1 frame before stimulus) and post-stimulus value (average of the 2-3 frames spanning the peak of the stimulus evoked response) was divided by the pre-stimulus value.

Note that in the case of DAN population imaging (Figures 2, 3 and S2), the DANs exhibit strong fluctuations in their basal activity, making it inaccurate to define a single absolute baseline F_0. The F_0 values used in the heatmap images are therefore simply the immediate pre-stimulus average, as described above, and should not be interpreted as a true minimum baseline. Indeed, because all DAN populations appeared to fluctuate between high and low activity states, the representative traces and stimulus-triggered averages for DAN population activity were all normalized between 0 and 1, where 0 represents the minimum fluorescence of the DAN compartment during a trace and 1 represents the maximum. Raw fluorescence traces of DAN activity depicting the relative levels of activation due to different stimuli are presented in Figure S2A. The normalized DAN activity data was used to measure the integrated basal activity in Figure S2D. As a consequence, we potentially underestimate the differences between basal signals in each DAN population, as the raw intensities in γ2- γ3 were generally higher than those in γ4- γ5 (data not shown).

Stimulus-Triggered Averages (Figures 2 and 3)
The normalized time series of sytGCaMP fluorescence in each compartment were aligned to the time point when the stimulus was applied for each replicate. In the case of Figure 2E, the 'stimulus' refers to the time point at which bouts of leg flailing started and stopped, as identified in the fly motion traces and confirmed by manual video analysis. Traces beginning 5 seconds before the stimulus and ending 5 seconds after the stimulus were averaged and displayed.

Cross-correlation Analysis (Figures 2D and S2B-S2C)*:*
Motion-tracking data was aligned to functional imaging data as described above. Pearson product-moment correlation coefficients between pairs of DANs and between individual DANs and motion were calculated for a 60-120 second recording in each animal. The resulting correlation coefficients were averaged and used to generate the cross-correlogram shown in the figures. Data in Figure S2B was calculated from individual traces in the same animal.

Statistical Analysis
Statistical analysis was performed using custom scripts in Excel and R. The significance of all results was tested by ANOVA followed by 2-tailed T-tests with Holm-Bonferroni post-hoc correction for multiple comparisons. Paired T-tests were used for changes in DAN activity due to all stimuli (Figures 2-3, Table S1), compartmental differences (Figures 4C-D, S4D-G), KC changes due to DAN activation or sugar feeding (Figures 5A-5C), MBON activity differences and changes (Figures 6, 7, S6C, S7), DAN basal activity differences (Figure S2D), and comparison of KC spiking due to current injection (Figure S6B). Unpaired T-tests were used for DopR/dDAT mutant/RNAi data (Figures 5D-E, and S5C-S5E) and comparisons of EPSC amplitudes due to optogenetic DAN activation (Figure S6A). To measure the significance of changes in DAN activity within each compartment due to exogenous stimuli or changes in behavioral state (Figures 2-3), DAN activity values were calculated by averaging the fluorescence intensity for 5 frames prior to the stimulus and for the 5 frames spanning the peak of the stimulus evoked response. The same windows were used for all compartments and all individuals within each panel. Changes within

each compartment were then measured by paired-T-test (Table S1). In some experiments (as indicated), each mushroom body of an animal was treated as an independent sample.

Optogenetic Activation of DANs (Figure S6A)
Flies expressing ReaChR, a red-shifted channelrhodopsin variant, in DANs using 58E02-LexA, LexAOP-ReaChr transgenes, were placed on food containing 400 μM all-trans retinal, a ReaChR cofactor, for 18-36 hours prior to dissection. Targeting of the γ4 MBON soma was carried out under fluorescence guidance, using the minimum possible intensity and duration of illumination by a 490 nm LED. Nevertheless, upon initiation of whole-cell recording, we observed that γ4 MBONs exhibited significantly larger excitatory postsynaptic potentials (EPSPs) and excitatory postsynaptic currents (EPSCs) when the 58E02-LexA, LexAOP-ReaChr transgenes were present in comparison to control animals lacking ReaChr expression. This observation suggests that ReaChr stimulation during dissection of the brain from its capsule under white light LED illumination and targeting of the γ4 MBON soma under fluorescence illumination is sufficient to activate DANs and alter properties of synaptic transmission.

Larval NMJ Immunostaining (Figure S1G)
Wandering third instar larvae were fileted in PBS. Dissected larvae were fixed for 2 min in Bouin's solution (Sigma) then rinsed with PBS 4 times and blocked in 5% Normal Goat Serum in PBS + 0.1% TritonX-100 for 2 hours at RT. Primary antibody 1:250 mouse anti-DCSP-2 (6D6) (Developmental Studies Hybridoma Bank), 1:50 mouse anti-Bruchpilot (NC82) (Developmental Studies Hybridoma Bank) and 1:10,000 rabbit anti-GFP (Life Technologies A-11122) was incubated overnight 4°C. Larvae were washed extensively in PBS + 0.1% TritonX-100 then incubated for 2 hours at RT with 1:400 goat anti-mouse Alexa Fluor 633 (Life Technologies A-21052), 1:400 goat anti-rabbit Alexa Fluor 488 (Life Technologies A-11034) and 1:500 Rhodamine Red-X conjugated goat anti-Horseradish Peroxidase (Jackson ImmunoResearch Laboratories 123-295-021). Larvae were then washed extensively in PBS + 0.1% TritonX-100 and mounted in Vectashield (Vector Laboratories). Images were captured on a Zeiss LSM 880 using a Plan-Apochromat 40X (1.4 NA) Oil DIC objective.

Adult Brain Immunostaining (Figure S4B)
Day 1 adult brains were dissected in 1X PBS pH 7.4 then immediately transferred to cold 1% PFA (Electron Microscopy Sciences) and fixed overnight at 4ºC. Following overnight incubation samples were washed in PAT3 Buffer (0.5% BSA/0.5% Triton/1X PBS pH 7.4) 3 times. Brains were blocked in 3% Normal Goat Serum for 90 minutes at RT. Primary antibody 1:1000 rabbit anti-GFP (Life Technologies A-11122) was incubated 3 hours at RT then overnight at 4°C. Brains were washed extensively in PAT3 Buffer. Secondary antibody 1:400 goat anti-rabbit Alexa Fluor 488 (Life Technologies A-11034) was incubated 3 hours at RT then 5 days at 4°C. Brains were washed 3 times in PAT3 Buffer then once in 1X PBS. Samples were mounted in Vectashield (Vector Laboratories). Images were captured on a Zeiss LSM 880 using a Plan-Apochromat 20X DIC objective.

RNA Isolation and qRT-PCR (Figure S5B)
Total RNA was isolated from dissected brains of day 1 adult females. RNA was extracted using Qiazol reagent (QIAGEN) then column purified by RNeasy micro kit (QIAGEN). cDNA was generated using Quantitect Reverse Transcriptase kit (QIAGEN). Taqman real-time qPCR experiments were performed on a QuantStudio 12K Flex Real-Time PCR System (ThermoFisher Scientific) following the manufacturer's instructions. Data were analyzed using the comparative $2\Delta\Delta C$t method using alphaTub84B as an endogenous control. The average fold-change relative to the pan-neuronal nsyb-GAL4 driver line alone was calculated. The following Taqman assays from ThermoFisher Scientific were used: *alphaTub84B* (Dm02361072_s1), *DopR1 (*Dm02134814_m1), *DopR2 (*Dm02151745_m1), and *D2R (*Dm01845575_m1).

Electrophysiology (Figures 6A and S6A-S6B)
γ4 MBON and KC soma were targeted for patch recording by fluorescence from expression of soluble GCaMP or CD8-GFP. Dissected brain explants were treated with 2 mg mL^{-1} collagenase (Sigma) in external saline for ~30 sec to soften the perineural sheath and pinned to a Sylgard sheet. The exposed neuropil was then continuously perfused (about 2–3 mL min^{-1}) with perfusion saline (108 mM NaCl, 5 mM KCl, 2 mM $CaCl_2$, 8.2 mM $MgCl_2$, 26 mM $NaHCO_3$, 1 mM NaH_2PO_4, 5 mM trehalose, 5 mM sucrose, 5 mM HEPES, osmolarity adjusted to 275 mOsm). The perfusion saline was continuously bubbled with

95% O_2/5% CO_2 and reached a final pH of 7.3. To gain access to the soma, the sheath was broken by positive pressure from ejection of saline through a large bore broken electrode.

Intracellular recordings were performed with fire-polished patch electrodes (10–15 MΩ for MBONs, 15-20 MΩ for KCs) filled with internal saline (130 mM potassium aspartate, 8 mM KCl, 0.2 mM $MgCl_2$, 5 mM sucrose, 10 mM HEPES pH 7.3, 10 mM EGTA). Current traces were acquired in voltage-clamp mode (for MBONs and KCs) and current-clamp mode (for KCs) using a Multiclamp 700B amplifier, digitized at 10 kHz and filtered at 1 kHz. The membrane potential of voltage clamp recordings was nominally -70 mV, a voltage at which unclamped action potentials rarely break through and could be readily detected by their large amplitude. Evoked EPSCs were stimulated by acetylcholine iontophoresis into the calyx as described above. For each experiment, the responses to a train of 10 identical stimulation voltages, spaced 3 s apart were recorded before and after DAN activation. The data plotted in Figure 6A are the peak amplitude from stimulus-triggered averages for each experiment before and after DAN activation. In rare cases where stimulation evoked MBON spikes despite the voltage clamp, those responses were excluded from the average. We note that EPSC durations are likely exaggerated by low-pass filtering due to the high access resistance (50-100 MΩ) common to whole-cell recordings from *Drosophila* neurons (Murthy and Turner, 2013b).

In Figure S6A, spontaneous EPSCs from 30-60 s traces (1 per fly) were analyzed in Clampfit (Molecular Devices), using a template search algorithm, with the template defined by the prominent EPSCs in the modulated MBON prep. As EPSCs in the unmodulated state were sometimes too small for reliable detection, this template search algorithm likely results in an underestimate in the difference in EPSC amplitude due to DAN stimulation.

To confirm that the spontaneous ESPCs measured in the MBON originated from KC activity (Figure S6A), we filled a fine electrode with 0.2 M GABA in external saline. After recording baseline EPSCs, the GABA electrode was moved from a position within the perfused saline to within the center of the mushroom body calyx. No further positive pressure was required to eject GABA. GABA applied in this manner rapidly inhibited measured EPSCs and EPSPs but did not suppress occasional spontaneous spiking in the MBON in current clamp recordings (data not shown.)

	γ2 DANs	γ3 DANs	γ4 DANs	γ5 DANs
Sugar	0.020684751	0.038021709	0.035413261	4.16266E-05
Shock	8.5723E-05	2.20578E-07	0.008606605	0.000795113
Flail	1.21501E-11	2.568E-10	0.044450088	5.11192E-06
Still	8.37411E-12	5.51872E-12	0.036962279	6.16218E-07
58E02-DANs> P2X2	1.07325E-09	0.61686413	3.94375E-07	1.56546E-08
γ2 DAN>P2X2	0.009663704	6.87552E-09	2.06957E-06	6.71104E-06
γ3 DAN>P2X2	0.000321854	0.000103841	1.19609E-05	3.48101E-07
γ4 DAN>P2X2	0.000161199	0.001572201	6.61172E-06	1.29759E-05
γ5 DAN>P2X2	0.013657448	6.42053E-05	3.52496E-05	0.000246935

Table S1.

Related to Figures 2 and 3.

p-values from paired T-tests comparing fluorescence intensities in DANs of each compartment before and after each stimulus shown in Figures 2 and 3.

Supplemental References

Chen, T.W., Wardill, T.J., Sun, Y., Pulver, S.R., Renninger, S.L., Baohan, A., Schreiter, E.R., Kerr, R.A., Orger, M.B., Jayaraman, V., et al. (2013). Ultrasensitive fluorescent proteins for imaging neuronal activity. Nature *499*, 295–300.

Chen, Y., Akin, O., Nern, A., Tsui, C.Y.K., Pecot, M.Y., and Zipursky, S.L. (2014). Cell-type-specific labeling of synapses in vivo through synaptic tagging with recombination. Neuron *81*, 280–293.

Connolly, J.B., Roberts, I.J., Armstrong, J.D., Kaiser, K., Forte, M., Tully, T., and O'Kane, C.J. (1996). Associative learning disrupted by impaired Gs signaling in Drosophila mushroom bodies. Science *274*, 2104–2107.

Friggi-Grelin, F., Coulom, H., Meller, M., Gomez, D., Hirsh, J., and Birman, S. (2003). Targeted gene expression in Drosophila dopaminergic cells using regulatory sequences from tyrosine hydroxylase. J. Neurobiol. *54*, 618–627.

Gibson, D.G. (2009). Synthesis of DNA fragments in yeast by one-step assembly of overlapping oligonucleotides. Nucleic Acids Res. *37*, 6984–6990.

Gordon, M.D., and Scott, K. (2009). Motor control in a Drosophila taste circuit. Neuron *61*, 373–384.

Inagaki, H.K., Jung, Y., Hoopfer, E.D., Wong, A.M., Mishra, N., Lin, J.Y., Tsien, R.Y., and Anderson, D.J. (2014). Optogenetic control of Drosophila using a red-shifted channelrhodopsin reveals experience-dependent influences on courtship. Nat. Methods *11*, 325–332.

Ishikawa, D., Takahashi, N., Sasaki, T., Usami, A., Matsuki, N., and Ikegaya, Y. (2010). Fluorescent pipettes for optically targeted patch-clamp recordings. Neural Networks *23*, 669–672.

Ito, K., Suzuki, K., Estes, P., Ramaswami, M., Yamamoto, D., and Strausfeld, N.J. (1998). The organization of extrinsic neurons and their implications in the functional roles of the mushroom bodies in Drosophila melanogaster Meigen. Learn. Mem. *5*, 52–77.

Jenett, A., Rubin, G.M., Ngo, T.T.B., Shepherd, D., Murphy, C., Dionne, H., Pfeiffer, B.D., Cavallaro, A., Hall, D., Jeter, J., et al. (2012). A GAL4-driver line resource for Drosophila neurobiology. Cell Rep. *2*, 991–1001.

Keleman, K., Vrontou, E., Krüttner, S., Yu, J.Y., Kurtovic-Kozaric, A., and Dickson, B.J. (2012). Dopamine neurons modulate pheromone responses in Drosophila courtship learning. Nature *489*, 145–149.

Kohatsu, S., Koganezawa, M., and Yamamoto, D. (2011). Female contact activates male-specific interneurons that trigger stereotypic courtship behavior in Drosophila. Neuron *69*, 498–508.

Li, H., Chaney, S., Forte, M., and Hirsh, J. (2000). Ectopic g-protein expression in dopamine and serotonin neurons blocks cocaine sensitization in Drosophila melanogaster. Curr. Biol. *10*, 211–214.

Murthy, M., and Turner, G. (2013a). Dissection of the head cuticle and sheath of living flies for whole-cell patch-clamp recordings in the brain. Cold Spring Harb. Protoc. *8*, 134–139.

Murthy, M., and Turner, G. (2013b). Whole-cell in vivo patch-clamp recordings in the drosophila brain. Cold Spring Harb. Protoc. *8*, 140–148.

Pitman, J.L., Huetteroth, W., Burke, C.J., Krashes, M.J., Lai, S.L., Lee, T., and Waddell, S. (2011). A pair of inhibitory neurons are required to sustain labile memory in the drosophila mushroom body. Curr. Biol. *21*, 855–861.

Riemensperger, T., Völler, T., Stock, P., Buchner, E., and Fiala, A. (2005). Punishment prediction by dopaminergic neurons in Drosophila. Curr. Biol. *15*, 1953–1960.

Tempel, B.L., Bonini, N., Dawson, D.R., and Quinn, W.G. (1983). Reward learning in normal and mutant Drosophila. Proc. Natl. Acad. Sci. U. S. A. *80*, 1482–1486.

Tully, T., and Quinn, W.G. (1985). Classical conditioning and retention in normal and mutant Drosophila melanogaster. J. Comp. Physiol. A. *157*, 263–277.

Wu, J.S., and Luo, L. (2006). A protocol for mosaic analysis with a repressible cell marker (MARCM) in Drosophila. Nat. Protoc. *1*, 2583–2589.

Yao, Z., Macara, A.M., Lelito, K.R., Minosyan, T.Y., and Shafer, O.T. (2012). Analysis of functional neuronal connectivity in the Drosophila brain. J. Neurophysiol. *108*, 684–696.